JOURNAL OF GUIDANCE, CONTROL, AND DYNAMICS
Vol. 24, No. 6, November–December 2001

Influence of a Small End Mass on Tether-Mediated Orbital Injection

Manuel Ruiz* and Jesús Peláez†
Universidad Politécnica de Madrid, 28040 Madrid, Spain

The tether-assisted slingshot injection allows raising the apogee up to about 14 tether lengths, depending on the angular speed, whereas the perigee only rises by one tether length. With a two-cut procedure, the tether departs with the satellite at the first cut and is discarded close to the apogee, so that the momentum transferred by the tether provides an additional raising of the perigee. This results in a longer lifetime. The disadvantages are that typical tethers are light and can transfer little momentum at the second cut and that libration with a free end is highly unstable. With zero tension at the tip, perturbations easily propagate and the rectilinear shape is lost. A modification is proposed that improves on both counts, leaving a mass attached to the free end of the tether. It can be part of the deployer assembly, so that no additional weight is needed. This increases the momentum transferred at the second cut, thus raising drag-sensitive perigee. Even small masses appreciably increase in lifetime. Tether tension is higher, so that libration is more stable and the rectilinear shape is preserved for a longer time. The new mass distribution changes the frequencies of the tether oscillations and can be used to avoid resonances.

Nomenclature

a	=	semimajor axis of the orbit of G, km
a_s	=	semimajor axis of the final orbit of S, km
a_{s1}	=	order one term of the expansion of a_s
B	=	tether end opposite to S
$E(\tau)$	=	time evolution of out-of-plane oscillations
e	=	eccentricity of the orbit of G
e_s	=	eccentricity of the final orbit of S
e_{s1}	=	order one term of the expansion of e_s
$\boldsymbol{e}$	=	Runge–Lenz vector
$F(\sigma, \tau)$	=	nondimensional tether tension
G	=	center of mass of the tethered satellite system
$G(t)$	=	time function in tether tension
H	=	scale height of exponential atmosphere, km
$H(\tau)$	=	coefficient in transverse oscillation equations
h_{ag}	=	apogee height of the orbit of G, km
h_{as}	=	apogee height of the orbit of S, km
h_{pg}	=	perigee height of the orbit of G, km
h_{ps}	=	perigee height of the orbit of S, km
$I_i(z)$	=	modified Bessel functions of the first kind
i	=	integer index
L	=	tether deployed length, km
M	=	satellite mass, kg
m	=	dead mass at tether end B, kg
n	=	mean orbital rate, $\sqrt{(\mu/a^3)}$, rad/s
O	=	deploying craft
$P(s)$	=	space function in tether tension
$P_n(x)$	=	Legendre polynomials
$Q_n(x)$	=	Legendre associated functions
R_O	=	radius of the circular orbit of O
$R(\nu)$	=	radius of the elliptic orbit of G
$\boldsymbol{r}_y^x$	=	position of body x at instant y
S	=	satellite
s	=	longitudinal abscissa along the tether, km
T_e	=	exospheric temperature, K
$T(s, t)$	=	tether tension, N
t	=	time, s
u	=	nondimensional angular rate θ' at the first cut, rad/rad
v	=	repeated expression
$\boldsymbol{v}_y^x$	=	speed of body x at instant y
x	=	variable for eigenfunction computation
$Z(\tau)$	=	time evolution of in-plane oscillations
z	=	variable for lifetime computation $a_s e_s/H$
β	=	tether length quotient, GS/OG
$\Delta(\cdot)$	=	increment of $(\cdot)$
δ	=	instant libration angle at the first cut
δ_a	=	ballistic coefficient times atmospheric rotation factor, kg/km^2
ϵ	=	small parameter $OG/2R_O$
ζ	=	in-plane transverse tether deviation
η	=	out-of-plane tether transverse deviation
θ	=	in-plane libration angle about local vertical
θ_M	=	in-plane libration amplitude before cuts
κ	=	shorthand for $1 + e\cos\nu$
λ_i	=	eigenvalues for transverse oscillations
μ	=	Earth's gravitational constant, km^3/s^2
ν	=	true anomaly of the orbit of G
ν_c	=	true anomaly of G at the second cut
ν_i	=	true anomaly of G at the first cut
ξ	=	longitudinal tether deviation
ρ	=	linear density of the tether, kg/km
ρ_p	=	air density at perigee, kg/km^3
σ	=	nondimensional tether abscissa, s/L
σ_{eq}	=	constant term in F
τ	=	nondimensional time nt, rad
Φ	=	eigenfunction for out-of-plane oscillations
ϕ	=	angle between EO and EG at the first cut
Ψ	=	eigenfunction for in-plane oscillations
Ω_E	=	Earth's angular speed
ω_O	=	orbital angular rate of O, rad/s

Superscripts

$\dot{(\cdot)}$	=	$\mathrm{d}(\cdot)/\mathrm{d}t$ (lifetime) or $\mathrm{d}(\cdot)/\mathrm{d}\tau$ (stability)
$(\cdot)'$	=	$\mathrm{d}(\cdot)/\mathrm{d}\nu$ (lifetime) or $\mathrm{d}(\cdot)/\mathrm{d}\sigma$ (stability)

Received 27 April 2000; revision received 21 February 2001; accepted for publication 6 April 2001. Copyright © 2001 by the American Institute of Aeronautics and Astronautics, Inc. All rights reserved.

*Assistant Professor, Escuela Técnica Superior de Ingenieros Aeronáuticos, Pl. Cardenal Cisneros 3; mrd@faia.upm.es.

†Associate Professor, Escuela Técnica Superior de Ingenieros Aeronáuticos; jpelaez@faia.upm.es.

Introduction

MOMENTUM transfer is one of the most commonly proposed dynamic applications of tethers, both to inject satellites into higher orbits and to lower loads for reentry.[1] It has been considered as a midterm system for low Earth orbit (LEO) to geosynchronous orbit (GEO) transfers,[2,3] though the debris danger favor LEO applications, where the discarded tether reenters quickly. Different aspects of momentum transfer have been planned for Bistatic

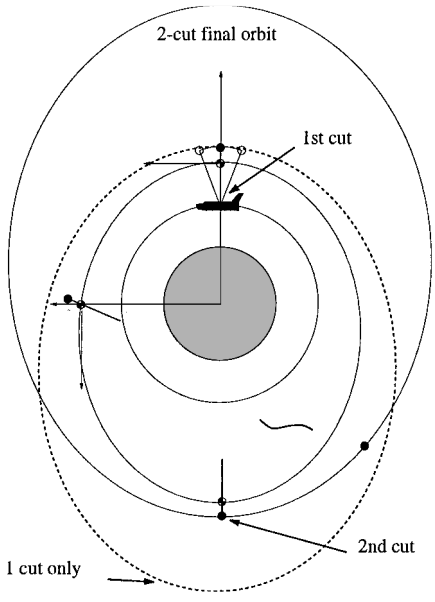

Fig. 1 Two-cut slingshot injection.

Observations using Low Altitude Satellites,[4] Advanced Tether Experiment, Young Engineers' Satellite, and Students for the Exploration and Development of Space Satellite.[5] They did not go ahead as planned for different reasons,[6,7] but not because of any fault of the momentum transfer concept, which remains valid.

Assume that a light satellite is tether-deployed zenithward from a massive craft in a circular orbit. Swinging the tether can raise the satellite apogee up to $7+4\sqrt{3}$ times the tether length L, but the perigee raise is limited to L. Rotation, if allowed by the deployer, can raise the apogee further, but not the perigee. This is often cited as the $14L$ rule.[1,8,9]

The two-cut slingshot injection intended for the original SEDSAT mission, shown in Fig. 1, is an improvement. The tether is cut at the lower end, leaving tether and satellite to librate as a gravity-gradient pendulum about the center of mass orbit. Close to the apogee, the tether is cut again, transferring additional momentum to the satellite. Apogee height decreases. The $14L$ rule is now applied to the orbiter to center of mass height, which is smaller than the orbiter-to-satellite height, but drag-sensitive perigee height rises. Now the $14L$ rule is applied to the center of mass-to-satellite length, instead of raising just L.

This procedure is ideal for a low-cost, small satellite launched as a secondary payload, such as Universidad Politécnica de Madrid's satellite.[10] Mission objectives can be reached from an orbit determined by the primary payload. However, the perigee and lifetime raise from the second cut is limited by the low mass of the typical tether.[11–13] Also, tethered satellite system (TS) libration with a free end is unstable, so that after some time the second cut is useless: The tether is no longer straight, and the momentum transfer is unpredictable.[13,14]

For a given tethered system, the process is characterized by three parameters: in-plane libration amplitude before the first cut, θ_M; instant libration angle at the first cut, δ; and true anomaly of the center of mass orbit at the second cut, ν_c. Their effect on satellite lifetime has also been studied.[12]

This paper proposes a modification of the process: Leave a mass attached to the lower end of the tether. It could be a part of the deployer, such as the brake/cut assembly. This has two effects:

1) It lowers the apogee and raises the perigee.

2) It improves the stability of the transverse oscillations in pendular motion.

An additional free parameter appears, namely, the end mass m. The aim of this study is to determine the combination of parameters leading to maximum life and stable librational motion.

Orbital Injection

A satellite S has been deployed from a massive craft O in a circular orbit about a spherical Earth. The deployment strategy for a desired

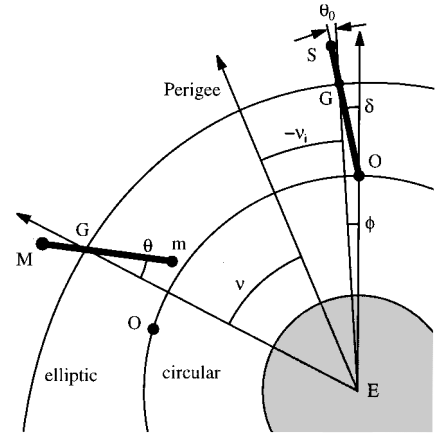

Fig. 2 Angles before and after first cut.

libration or spin has been studied[9,15] and will not be considered here. The mass of TS $(M+\rho L+m)$ is small, so that the orbit of O is not perturbed. No out-of-plane libration will be considered because its effect for small amplitudes has been found to be negligible.[9] The in-plane libration of the TS about the local vertical of O is governed by the well-known equation[14,16]

$$\dot{\theta}^2 + 3\omega_O^2 \sin^2\theta = 3\omega_O^2 \sin^2\theta_M \tag{1}$$

When $\tau = \omega_O t$ is introduced as variable, $\dot{\theta}$ will become the nondimensional angular speed θ'. Setting and notation are shown in Fig. 2. When the tether is cut, the center of mass G of the TS stops librating about O and enters a higher, elliptic orbit. If cut at a libration angle $\theta = \delta$, the TS is left with a nondimensional angular rate $u = \sqrt{3}\sqrt{(\sin^2\theta_M - \sin^2\delta)}$. This angular rate is measured about the local vertical of O, but the TS now librates as a gravity-gradient pendulum about the new local vertical EG. The governing equation is obviously more complex[14,16]:

$$(1+e\cos\nu)\frac{\mathrm{d}^2\theta}{\mathrm{d}\nu^2} - 2e\sin\nu\left(1+\frac{\mathrm{d}\theta}{\mathrm{d}\nu}\right) + 3\sin\theta\cos\theta = 0 \tag{2}$$

Note that now θ is different due to the new local vertical, and true anomaly ν is also different from the anomaly $\omega_O t$ of the circular orbit. Initial conditions need adjustment to account for the new reference frame. Taking true anomaly as variable simplifies the integration because the use of time requires solving the Kepler equation at each integration step.

At a certain value of the anomaly ν_c, the tether is cut again, and the satellite enters its final orbit, and the tether and end mass are supposed to go into a lower orbit and reenter. The free parameters θ_M, δ, ν_c, and m, plus the system configuration L, M, ρL, and R_O, fully determine the orbit of G and the final orbit of S:

1) The orbital speed of O, δ, and Eq. (1) determine the speed and position of G and, thence, its orbital parameters and initial anomaly ν_i, as shown in Fig. 2.

2) After some adjustments due to the change of reference frame and variable, δ and u give the initial conditions to integrate numerically Eq. (2) from ν_i to ν_c.

3) The position and speed of S (and thus the satellite final orbit a_s, e_s) are given by ν_c, $\theta(\nu_c)$, and $\theta'(\nu_c)$.

Following these steps, a straightforward numerical routine can be written to obtain the final orbital elements as a function of the cut parameters. It will be used later to find the parameters leading to maximum lifetime. Nevertheless, an analytical solution would give some insight on the influence of each parameter. Because $L \ll R_O$, an expansion in powers of $\epsilon = OG/2R_O \ll 1$ leads to approximate expressions for the orbital elements of the TS and, afterward, of the satellite.[12,13,17] This requires a symbolic algebra program such as Maple V. At the time of the first cut, the position of G is

$$\boldsymbol{EG} = \boldsymbol{r}_0^G = R_O\{1+2\epsilon\cos\delta,\, 0,\, 2\epsilon\sin\delta\}$$

where the x axis is EO and the z axis is orthogonal and contained in the orbital plane. When orbital motion and libration are taken into account, the speed of G is

$$\boldsymbol{v}_0^G = \omega_0 R_0\{-2(1+u)\epsilon\sin\delta,\, 0,\, 1+2(1+u)\epsilon\cos\delta\}$$

The angular momentum per unit mass, $\boldsymbol{h} = \boldsymbol{r}_0^G \wedge \boldsymbol{v}_0^G$, can now be obtained, and then the Runge–Lenz or eccentricity vector $\boldsymbol{e}$, whose modulus is the orbital eccentricity, can be obtained. Energy is also computed, leading to an expression for the semi-axis a. Explicit approximate expressions can be obtained through a Taylor expansion in the small parameter ϵ:

$$a = R_O\{1 + 4\cos\delta(u+2)\epsilon + 4[\cos^2\delta(13 + 16u + 4u^2) + 2 + 2u + u^2]\epsilon^2 + \cdots\}$$

$$e = 2v\epsilon + 2\cos\delta\{[(\cos^2\delta + 1)(9 + 18u + 12u^2 + 2u^3) - 2u^2]/v\}\epsilon^2 + \cdots$$

where, for brevity, $v = \sqrt{[3\cos^2\delta(u+1)(u+3) + u^2]}$. For G, the apsidal height increases in the intermediate orbit are, to first order,

$$\Delta h_{\text{pg}} = a - ae - R_O = 2R_O[2\cos\delta(u+2) - v]\epsilon + o(\epsilon)$$

$$\Delta h_{\text{ag}} = a + ae - R_O = 2R_O[2\cos\delta(u+2) + v]\epsilon + o(\epsilon)$$

First cut optimization is straightforward because both are maximum when $\theta_M = \pi/2$ and $\delta = 0$, yielding the $14L$ rule.

For the final orbit, the libration equation must be numerically integrated to obtain the position and speed of the satellite at $\nu = \nu_c$. This requires computing the initial conditions after the first cut and adjusting for the change in reference frames.

The initial anomaly measured from perigee is computed as

$$\sin\nu_i = \frac{\boldsymbol{r}_0^G \wedge \boldsymbol{e}}{|\boldsymbol{r}_0^G| \cdot |\boldsymbol{e}|} \cdot \boldsymbol{j}$$

where $\boldsymbol{j}$ is the unit vector along the normal to the orbital plane and is used to find the initial orbital angular speed $\dot{\nu}_0 = n(1 + e\cos\nu_i)^2(1 - e^2)^{-3/2}$. The latter leads to the initial libration angular speed through a composition of motions between the elliptic and the circular orbits and their respective librations: $\dot{\theta}_0 = u + \omega_O - \dot{\nu}_0$. Dividing by $\dot{\nu}_0$, we obtain the nondimensional libration angular speed θ_0', where true anomaly is taken as variable. The initial libration angle, on the other hand, is straightforward: $\theta_0 = \delta - \phi$. Here, θ_0' and θ_0 obviously refer to the local vertical of the orbit of G.

With these initial conditions, numerical integration of Eq. (2) leads to the libration angle and speed at the second cut, θ_c' and θ_c. The position of the satellite is, therefore,

$$\boldsymbol{r}_c^S = \{R(\nu_c) + 2\epsilon\beta R_O\cos\theta_c, 0, 2\epsilon\beta R_O\sin\theta_c\}$$

where the orbital radius $R(\nu_c)$ is easily computed with a, e, and ν_c and where β is the tether length quotient. The satellite speed includes the effect of the orbit and of the libration:

$$\boldsymbol{v}_c^S = \dot{\nu}_c(\theta_c' + 1)2\beta\epsilon R_O\{-\sin\theta_c, 0, \cos\theta_c\} + an\{e\sin\nu_c, 0, 1 + e\cos\nu_c\}\Big/\sqrt{1 - e^2}$$

As in the first cut, position and speed are used to compute the final orbit of the satellite. When expanding in ϵ, approximate expressions can be obtained for all terms except θ_c' and θ_c, leading to the following orbital elements:

$$a_s = R_0[1 + a_{s1}\epsilon + o(\epsilon)], \qquad e_s = e_{s1}\epsilon + o(\epsilon)$$

where

$$a_{s1} = 4\beta\cos\theta_c(2 + \theta_c') + 4\cos\delta(2 + u)$$

$$e_{s1} = \Big\{[2\beta\cos\theta_c(3 + 2\theta_c') + 2v\cos\nu_c]^2 + (2\beta\theta_c'\sin\theta_c - 2v\sin\nu_c)^2\Big\}^{\frac{1}{2}}$$

These explicit expressions allow some conclusions on the qualitative effect of each free parameter. Because life will be longer when a_s is high and e_s low, the optimization of the second cut would call for $\nu_c = 3\pi$, $\theta = 0$, and θ' positive. Equation (2) shows that θ' then reaches its maximum, close to $\sqrt{3}$. In this case, $\nu_c = \pi$ is ruled out because numerical integration shows that $\theta' < 0$, as can be seen in Fig. 3. The optimization of the first cut called for $\theta_M = \pi/2$, $\delta = 0$, and $u = \sqrt{3}$.

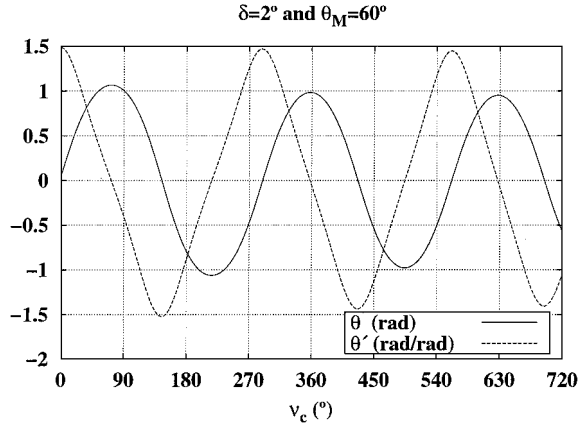

Fig. 3 Libration angle θ and rate θ'.

With these ideal values, the final apsidal height increases would be

$$\Delta h_{\text{ps}} = OG + \left(7 + 4\sqrt{3}\right)GS, \qquad \Delta h_{\text{as}} = \left(7 + 4\sqrt{3}\right)OG + GS$$

which correspond to the application of the $14L$ rule to the second cut as well. At first sight, a_s depends on β and ϵ. However, these two parameters are related in such a way that a_s depends basically on L, and β, the mass distribution, has only a marginal effect. Note that e_s does depend on β, becoming 0 when $\beta = 1$; this suggests that $m = M$ would lead to circular orbit and maximum life. In that case, the two cuts would have the same effect. For $\beta > 1$, the perigee and apogee swap places.

However, the ideal conditions cannot be met all at the same time. The first cut optimum values cannot be reached: Beyond $\theta_M \simeq 65.5$ deg in circular orbit[16] or $\simeq 63$ deg in elliptic orbit,[14] tension falls to zero. Beyond that, a rigid body in pendular motion would have to withstand compression. For a flexible tether, the equations no longer apply: It would crumple and lose the rectilinear shape. As for the second cut, θ and θ' are not free. They are given by Eq. (2) for each ν_c, and the two frequencies are not commensurable.

Because the optimum values are unreachable and height increases only give general orientations, an explicit computation of lifetime is needed.

Lifetime

For a spherical, rotating, exponential atmosphere with constant scale height H and a low eccentricity orbit ($e_s < 0.02$), King-Hele gives a lifetime estimation[18]:

$$t_L = \frac{He^z I_0(z)\{1 + 2e_s[I_1(z)/I_0(z)] - 9e_s z/40 + H/2a_s\}}{\delta_a\rho_p\sqrt{a_s\mu}[I_0(z) - I_2(z)][I_0(z) + 2e_s I_1(z)]} \tag{3}$$

The satellite ballistic coefficient includes an atmospheric rotation factor, $\delta_a = (A_s C_D/M)(1 - \cos i\Omega_E/n)^2$.

This expression can be plotted as a function of a_s and e_s showing that, as surmised, for constant a_s maximum life corresponds to $e_s = 0$; however, within the expected range, sensitivity to a_s is much greater than sensitivity to e_s.

The Cosmo and Lorenzini atmospheric model[1] will be used, which gives simple expressions for ρ_p and H as functions of height and exospheric temperature. Because a general study cannot account for solar activity variation, an average value will be taken, namely, $T_e = 900$ K. For specific satellites, launch timing within the solar cycle will affect actual lifetime values, but the optimization results will still apply.

The values originally considered for SEDSAT will be taken as representative of a small satellite launched from the shuttle: $M = 32$ kg, $L = 20$ km, $\rho L = 6.6$ kg, $R_O = 6675.39$ km, $i = 57$ deg, and $A_s C_D/M = 118 \cdot E6$ kg/km^2.

When the steps outlined in the preceding section are followed and Eq. (3) is used, lifetime is computed as a function of the cut parameters, leaving m free. A multivariate conjugate-gradient numerical maximization[19] is performed, giving the set of parameters leading to maximum lifetime for each value of m. Maximum life and corresponding apsidal height increments are shown in Fig. 4 together with ideal values. As expected, ideal maximum corresponds to $m = M$, or circular orbit. The real maximum corresponds to a slightly higher m and about 80% of the ideal life. The yield is even higher for lower m.

The cut parameters leading to maximum life are shown in Fig. 5. Maximum lifetime is reached with v_c very close to apogee. It doubles the value of the one-cut procedure. Better still, as m rises, optimum θ_M decreases, moving away from the zero-tension higher amplitudes.

It has been shown[12,13] that lifetime sensitivity to δ and θ_M is small, whereas sensitivity to v_c is high. Figures 4 and 5 show that sensitivity to m is also high. Note that δ and θ_M for maximum life do change with m, but for constant m lifetime is hardly affected by small changes in these angles. They can be chosen as 60 and 2 deg, optimum values for small m, which is the most likely case, leaving only v_c and m as free variables.

The apogee height thus obtained is shown in Fig. 6. It is always lower than with the one-cut procedure, where $G \equiv S$; as m increases, OG is shorter and apogee lower. Relative maxima are close to $\theta = 0$ and $\theta' > 0$, as shown in Fig. 3. The second is a little before perigee and benefits mostly apogee. The third is after apogee and benefits perigee height.

For perigee, the second cut is generally positive with very high peaks, as shown in Fig. 7. A heavier m means a longer GS and greater speed at the same rotation rate θ'. Maxima are also close to positive θ' and $\theta \simeq 0$; the second time it happens close to apogee and leads to maximum perigee height and lifetime. Note that the first apogee passage is bad both for h_a and h_p because θ' is negative and the satellite is thrown back.

The net effect on lifetime, as shown in Fig. 8, is negative most of the time, but remarkably positive, up to twice the one-cut life, near the second apogee passage. Sensitivity looks high in Fig. 8, but it is more reasonable once translated into time and even more so for lower m.

There are two aspects to lifetime increase in the second cut. First, the satellite must be launched forward and as fast as possible, which requires $\theta = 0$ and θ' maximum and positive, as shown in Fig. 3. Second, the launch must occur as close to apogee as possible, to maximize perigee height. If the two conditions are met, the absolute maximum life is attained (with the limitation imposed by low tension on θ_M). Thus, the two-cut injection would be analogous to a Hohmann transfer.

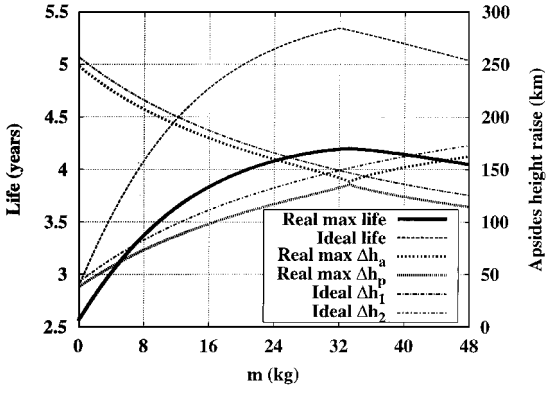

Fig. 4 Real maximum lifetime and ideal maximum.

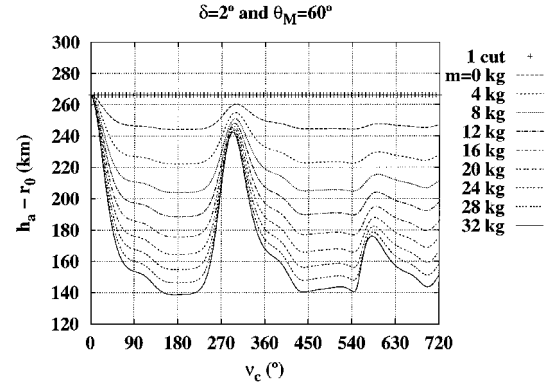

Fig. 6 Apogee raise of final satellite orbit.

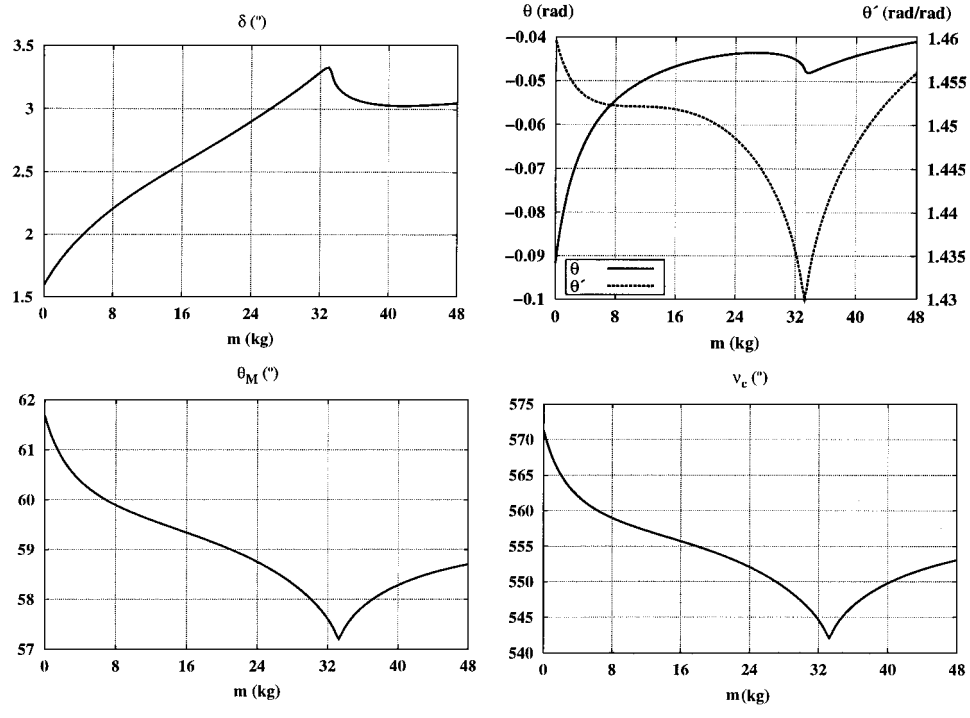

Fig. 5 Cut parameters for maximum lifetime.

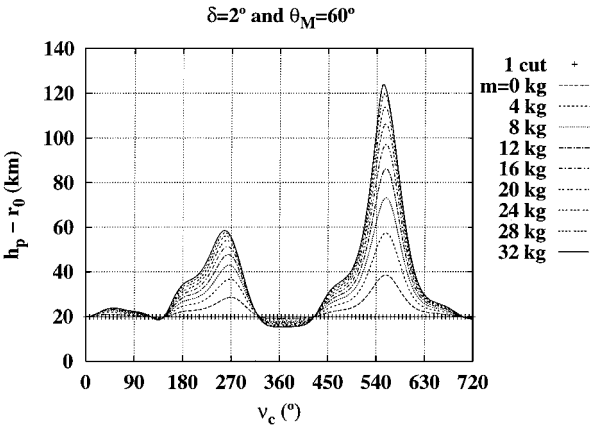

Fig. 7 Perigee raise of final satellite orbit.

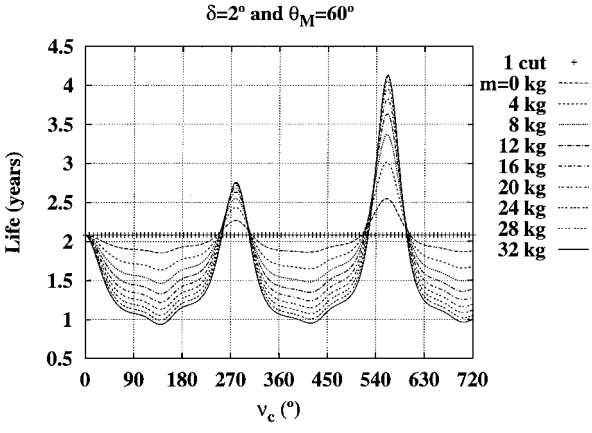

Fig. 8 Satellite lifetime for different values of end mass.

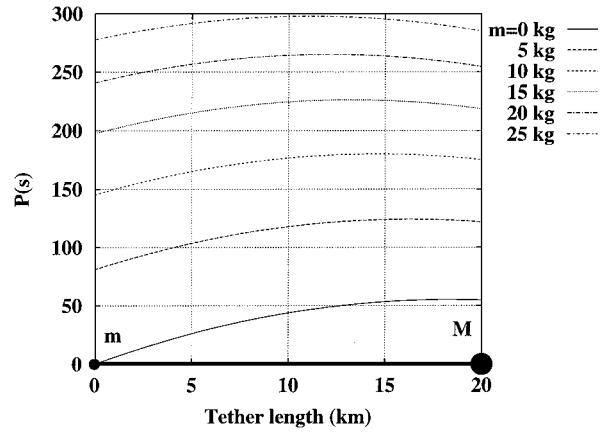

Fig. 9 Space-dependent tension distribution.

This absolute, ideal maximum occurs when the nodes of two noncommensurable oscillations coincide, namely, libration and orbital motion. They come arbitrarily close after a sufficiently long time. Note that only two orbits have been computed here, whereas higher lifetimes can be obtained by considering longer periods. This is not attractive, though, for two reasons. Atmospheric drag on the long tether, neglected here because the injection is assumed to take a short time, would meanwhile eat up more than the expected gain. Also, the tether will not remain straight for long because pendular motion in an elliptic orbit has been found to be unstable for a free-end tether.[14] It would soon twist and crumple, reducing the momentum transfer potential. This latter point deserves a more detailed study.

Stability of the Pendular Motion

Libration of a Flexible Tether

Between the first and the second cut, the TS is supposed to move as a rigid pendulum under gravity-gradient forces. Stability of libration of a rigid body in elliptic orbit has been studied by Schechter,[20] Modi and Brereton,[21] and Brereton and Modi.[22] Beletsky and Levin have studied the stability of the equilibrium configurations and the libration of a flexible tether in a circular orbit,[16] in the latter case, only for small libration amplitudes. Ruiz et al. have extended that analysis to the case of an elliptic orbit, large amplitudes, and a free end.[14] The full deduction is too long to be reproduced here because it would require a paper of its own, and we are interested here in the application rather than in the method. Nevertheless, an outline of the reasoning will be given.

Tether libration in an elliptic orbit can become unstable because of two factors: resonances between the orbit, the libration, and the different oscillation modes and loss of tension at high amplitudes, whereby the tether can adopt an arbitrary shape.[11,14] The combination of the two factors is especially dangerous because oscillation amplitude grows more easily with low tension. When one of the ends is free, as happens in the two-cut injection, tension is zero at that point and very low throughout the tether. Large oscillations can easily develop near the free end.

The equations governing in-plane pendular motion are well known[16]: libration is governed by Eq. (2); tether tension is a function of time and position along the tether, $T(s, t) = P(s)G(t)$, where $G(t)$ is a function of time through the libration angle and speed.[16] This can easily be obtained from the equilibrium of a tether element under tension, gravity forces, and inertial forces from the libration and orbital motion. Nondimensional variables can be introduced so that $T = \rho n^2 L^2 F(\tau, \sigma)$, with $F(\sigma, \tau) = P(\sigma)G(\tau)$. For a homogeneous tether, and taking the center of mass as origin of nondimensional abscissa σ, F can be easily integrated to yield[16]

$$F(\sigma, \tau) = \tfrac{1}{2}[(\dot{\theta} + \dot{\nu})^2 - (\dot{\nu}^2/\kappa)(1 - 3\cos^2\theta)]\left(\sigma_{\text{eq}}^2 - \sigma^2\right) \quad (4)$$

where dots are derivatives with respect to τ. The constant term in $P(\sigma)$, σ_{eq}, corresponds to half of the nondimensional tether length needed to have the same tension distribution without any end masses. Such a tether would have $\sigma_{\text{eq}} = \frac{1}{2}$ and a parabolic distribution of tension, with a maximum at the center, and falling to zero at the tips. When an end mass M is added, $\sigma_{\text{eq}}^2 = \sigma_S^2 - 2M\sigma_S/(\rho L)$, the maximum of the parabolic distribution goes to the center of mass, the free end keeps zero tension, and the end with a mass has a finite tension.

Figure 9 shows tension distribution $P(\sigma)$ for a 20-km tether with a fixed end mass $M = 32$ kg (right), as a function of the other end mass m (left). Note that the maximum moves toward the left with G as m increases. Even a small mass appreciably raises the tension at the end. This has a stabilizing effect by removing the whiplash effect of the free end and keeping the tether taut.

Note that the time-dependent factor $G(\tau)$ represents the centrifugal and gravity-gradient force at a unit distance from the origin.[16] When $G(\tau) = 0$, typically during the back swing, when θ' is negative, tension falls to zero throughout the tether, regardless of the mass distribution, which only affects $P(\sigma)$. When it becomes negative, the tether would have to withstand compression to keep moving as a pendulum. Because it cannot do that, it loses its rectilinear shape, and the equations are no longer valid.

Parametric resonances can be studied through the equations for small deviations from the rigid-body pendular libration.[13,14,16] A reference frame $G\xi\eta\zeta$ bound to the rigid TS is chosen, such that $G\xi$ is along the tether GS, $G\eta$ is normal to the orbital plane, and $G\zeta$ is within the orbital plane completing a right-handed frame. When the tether is no longer straight, the position vector of a tether element would be $\{s + \xi(t, s), \eta(t, s), \zeta(t, s)\}$. In this case, $\xi(t, s)$ corresponds to longitudinal oscillations, $\zeta(t, s)$ to in-plane transverse oscillations, and $\eta(t, s)$ to out of plane transverse oscillations. Note that the definition of ξ, just the perturbation, is different from that given by Beletsky and Levin,[16] which includes s.

Beletsky and Levin[16] write the equations of motion of a tether element in pendular libration axes $G\xi\eta\zeta$, whose motion is well known. When tension, gravity, and inertial forces are taken into account, a set of partial differential equations is obtained, coupled through the tension equation. For small oscillations, equations are linearized about

the pendular libration solution, leading to decoupled equations for each oscillation, longitudinal, transverse in-plane, and transverse out-of-plane. The longitudinal equation provides the main term of the tension, Eq. (4), which is used in the transverse equations. These are also decoupled and lead to a Sturm–Liouville problem. The spatial part gives the eigenvalues λ_i and eigenfunctions, and the time part gives the stability of each mode.

The time equations for η and ζ depend on time through the libration angle and speed, θ and $\dot{\theta}$, so that no analytical solution is possible. For small amplitude oscillations, however, $\theta(t)$ can be expressed as a trigonometrical function of t, and the time equations become Mathieu equations. Thus, Beletsky and Levin[16] study the stability of transverse oscillations about pendular libration through the Mathieu stability map in the variables $[\lambda_i, \theta_M]$, where periodic solutions are the boundary of the stable and unstable, or unbounded, solutions. Obviously, this analysis is only valid for small amplitudes, the mostly stable areas, close to the λ_i axis, whereas little can be said about the high libration amplitudes, where the instability areas are wider.

Eigenmodes

The authors have applied this approach to a tether librating in an elliptic orbit. The expressions are similar, except that the inertia forces correspond to an elliptic orbit, and libration is governed by Eq. (2) instead of Eq. (1). Also note that Beletsky and Levin[16] consider in-plane and out-of-plane libration, whereas here the out-of-plane libration angle is always zero. The nondimensional deviations from the pendular motion, $\xi(\tau, \sigma)$, $\eta(\tau, \sigma)$, and $\zeta(\tau, \sigma)$, are assumed to be small, for example, of order ϵ. Because the tension is low in the tether, it can be considered as inextensible. In any case, elastic longitudinal oscillations are easily damped by internal friction. Thus, the longitudinal deviations are just the result of the transverse oscillations, and the tether continuity equation shows that the longitudinal deviations are negative and one order of magnitude smaller than the transverse ones, or $\xi \simeq \epsilon^2$:

$$\sqrt{(1+\xi')^2 + (\eta')^2 + (\zeta')^2} = 1 \Rightarrow \xi' \ll \eta', \zeta' \tag{5}$$

When the perturbation of order $O(\epsilon^2)$ and higher are neglected, the longitudinal equation just gives the order zero term of the tension, which is used in the other two equations. [Carrying the order of magnitude of the derivative ξ' over to the function ξ could raise some doubts. However, substituting trigonometric functions $\sin(n\sigma/\pi)$ for η and ζ, the continuity equation (5) can be integrated for ξ in terms of elliptic functions. Thus, $\xi_{\max}(\eta_{\max}, \zeta_{\max})$ has a horizontal slope at the origin, which confirms the order of magnitude assumption.] Thus, the in-plane and out-of-plane transverse oscillations are decoupled, reducing to a Sturm–Liouville problem:

$$\ddot{\eta} = (F\eta')' - (\dot{\nu}^2/\kappa)\eta$$

$$\ddot{\zeta} = (F\zeta')' - [\dot{\nu}^2(3\sin^2\theta + e\cos\nu)/\kappa + 2\dot{\nu}\dot{\theta} + \dot{\theta}^2]\zeta \tag{6}$$

where F is the pendular libration nondimensional tension from Eq. (4), dots are derivatives with respect to τ, and primes are derivatives with respect to σ. When the functions $\eta = \Phi(\sigma)E(\tau)$, $\zeta = \Psi(\sigma)Z(\tau)$, and $F = G(\tau)P(\sigma)$ are introduced, the variables are separated, leading to

$$\frac{\ddot{E} + (\dot{\nu}^2/\kappa)E}{GE} = \frac{(P\Phi')'}{\Phi} = -\lambda_\eta$$

$$\frac{\ddot{Z} - HZ}{GZ} = \frac{(P\Psi')'}{\Psi} = -\lambda_\zeta \tag{7}$$

where $H(\tau)$ is the coefficient of ζ in Eqs. (6).

Space equations are the same for in-plane and out-of-plane deviations. Eigenvalues and eigenfunctions will be the same as well:

$$P\Psi'' + P'\Psi' + \lambda\Psi = 0 \tag{8}$$

They can be integrated numerically with the well known boundary conditions $\Psi''(\sigma_S) = 0$ and $\Psi''(\sigma_B) = 0$ at the end masses S and B (Ref. 16). Because the origin is the center of mass, the abscissas of the two ends are

$$\sigma_S = \frac{m + \rho L/2}{m + \rho L + M}, \qquad \sigma_B = -\frac{M + \rho L/2}{m + \rho L + M}$$

There is a singularity at B for $m = 0$, because P is zero and Ψ'' is not defined: The free end can have an arbitrary curvature. The only condition that can be imposed is that Ψ remain bounded, which is enough.

The change $x = \sigma/\sigma_{\text{eq}}$ leads to the Legendre differential equation, whose solution for integer λ is a combination of $P_n(x)$ (bound) and $Q_n(x)$ (∞ at ± 1). Also note that, at B, x is -1 when $m = 0$, raising the concern that the eigenfunctions could be singular at the free end.

At this stage, as in the case of the launch parameters, an analytical solution, though approximate, could give some insight on what is going on. In fact, λ will not be an integer; however, for light tethers, a perturbation method leads to a (rather involved) solution in terms of $P_n(x)$ and $Q_n(x)$. The details have already been described and need not be repeated here.[14] The small parameter is now $\overline{GS}$, which, for light tethers, is much smaller than L. Forcing the terms containing $Q_n(x)$ to be 0 at $x = -1$ yields the eigenvalues. Some coefficients are left unknown at each order equation and must be determined through compatibility conditions in the next order. The solution can be computed up to order $(\overline{GS}/L)^2$ and the compatibility conditions up to $(\overline{GS}/L)^3$; beyond that the algebra becomes too complex.

Nevertheless, this gives a cue for the numerical integration: The eigenvalues must be such that the eigenfunctions remain bounded at the free end. Integration can start from S with a seed value for λ obtained from the approximate perturbation solution. Because Ψ becomes ∞ at B for all λ except the real eigenvalue, a shooting method can find both. The algorithm used is described by Press et al.[19] When m is not zero, there is no singularity at B. The same shooting method can be used, but instead of Ψ being bounded at B, the condition is that $\Psi'' = 0$.

Numerical integration with either x or σ, thus, yields the eigenfunctions and eigenvalues; the latter are shown in Fig. 10 as a function of m, where λ_1 is 1 for all m. The others increase with m and with the mode number. This will reduce the amplitude of the oscillations of the higher modes and heavier m because the restoring term in the time equations (7) will be large, provided that $G(\tau) > 0$. As θ_M approaches the zero-tension zone beyond 63 deg, motion becomes unpredictable. The loose tether can take arbitrary shapes.

Eigenfunctions are shown in Fig. 11 for different values of m. A peculiar normalization, $\Psi(\sigma_S) = 1$, has been chosen to highlight the effect of the free end in the oscillations. Note that, as m grows, the shape of the eigenfunctions approaches the trigonometric functions typical of a tense string. As m decreases and becomes zero, the free end takes a dominant part in the overall oscillation. The zero-mass eigenvalues are very similar to Legendre polynomials, they are Legendre polynomials in the limit $M \to \infty$ or $\rho = 0$, and their shape retains the whiplash look of the free end motion.

In all cases, the first eigenfunction, associated with λ_1, is a straight line. As noted by Beletsky and Levin,[16] this mode is a perturbation of

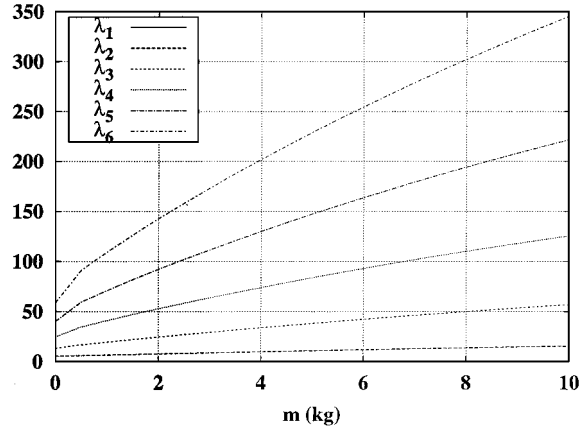

Fig. 10 First six eigenvalues vs *m*.

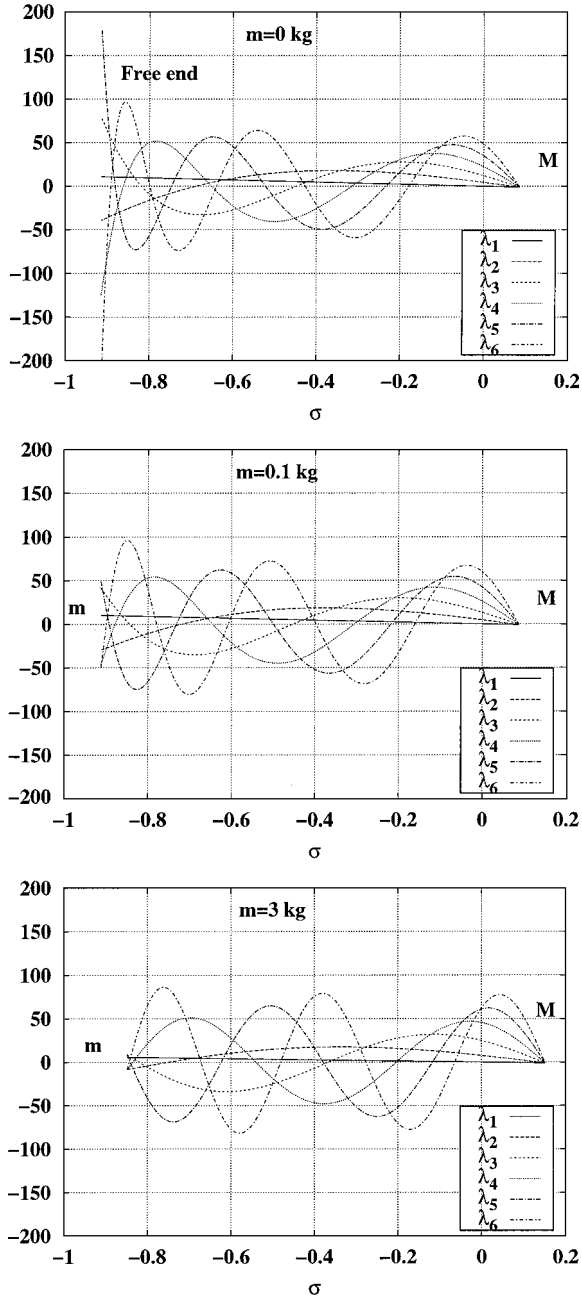

Fig. 11 Eigenfunctions for different m.

the underlying libration. When the time equations are integrated, this mode will always diverge, which is not surprising. Libration is not Lyapunov stable but is orbitally stable. A perturbation of the libration results in a different libration period, which, from the linearized motion, is seen as an unbounded growth. The order zero eigenmode mentioned by Beletsky and Levin, a horizontal line corresponding to a perturbation of the underlying orbital motion, does not appear here because the origin of the reference frame is always the center of mass of the TS.

Time Evolution and Stability

In the case studied by Beletsky and Levin,[16] approximate integration of small-amplitude libration led to Mathieu equations, whose stability is well known. This is not possible here. Equations (7) are still linear and homogeneous, but coefficients are more complex. First, orbital eccentricity appears in the coefficients directly or through κ. Second, the libration $\theta(\tau)$ cannot be approximated through $\sin\theta \simeq \theta$ because we are interested in the high amplitudes leading to maximum life. The full nonlinear equation must be solved. Therefore, the coefficients cannot be obtained explicitly. Time equations for each mode must be integrated numerically along with the libration equation.

Both the libration equation and the coefficients of the time equations explicitly include a true anomaly. This would require solving the Kepler equation at each step of the numerical integration. A better way is to take a true anomaly as an independent variable, as is already done in Eq. (2). Thus, Eqs. (7) and (2) become

$$\ddot{\theta} = (2e\sin\nu/\kappa)(\dot{\theta}+1) - (3/\kappa)\sin\theta\cos\theta$$

$$\ddot{E} = (2e\sin\nu/\kappa)\dot{E} - [\lambda_i G(\nu) + 1/\kappa]E, \qquad i = 1,\ldots,n$$

$$\ddot{Z} = (2e\sin\nu/\kappa)\dot{Z} - [\lambda_i G(\nu) - H(\nu)]Z, \qquad i = 1,\ldots,n \tag{9}$$

which must be numerically integrated with the appropriate initial conditions. The equations for all modes can be integrated in parallel with that of the libration because θ and ν are the same for all.

The structure of Eqs. (9) and the eigenvalues shown in Fig. 10 warrant some speculation on the behavior of the solutions, at least for small eccentricities, where their perturbing terms will be small save in the case of resonances. Higher modes have large eigenvalues, more so as the mass m increases, and, thus, have high restoring terms and frequencies, as long as $G(\tau) > 0$, that is, while tension is positive. Therefore, the higher modes are likely to be more stable, but all modes will diverge as we approach the low tension areas, which correspond to high libration amplitudes.

For this nonautonomous system, with perturbations from three different frequencies, orbital, libration, and each mode's, no analytical exploration of stability is feasible. We cannot ascertain whether the motion of a specific mode is Lyapunov stable, which would require integrating it for an infinite time. The most that can be done is to check that the amplitudes remain bounded for a reasonable time, a brute force approach, so that whatever maneuver is needed can be completed.

Because the system is homogeneous in the eigenmodes, a fundamental matrix is constructed with two independent solutions for each mode and direction: initial deviation, zero speed $[E_i(0)=1,\ \dot{E}_i(0)=0]$ and initial speed, zero deviation $[E_i(0)=0,\ \dot{E}_i(0)=1]$, both for in-plane ($Z$) and out-of-plane ($E$) oscillation. Six modes will be computed in this case, so that Eqs. (9) will have a total of 25 second-order equations. If at least one mode grows without bound, a distinctive exponential growth in the amplitude curves, the system will be unstable. If all remain bounded, the system will be stable for the time and modes computed, but nothing can be said about the long-term behavior.

This is done for different values of the initial libration amplitude θ_M and of the end mass m. The initial conditions for libration θ will be those of the optimum first cut, $\delta = 0$, with θ_M as a free variable. These cut parameters determine the orbit eccentricity as well. Note that for $\delta = 0$ the initial libration angles in the elliptic and circular orbits coincide, but their derivatives do not.

Numerical Results

In the case of the free end, $m = 0$, the first six eigenvalues λ_1–λ_6 are computed as stated. Equations (9) are numerically integrated for 100 orbits, for the first six modes, for in-plane Z and out-of-plane E oscillations, and for each of the two independent solutions initial speed and initial deviation. This is repeated for a range of θ_M from 51 to 61 deg because the higher amplitudes lead to maximum life. We should not go too high, though, because tension falls to zero at some point between 63 and 64 deg.

For each mode, the maximum elongation E or Z in each period is recorded, so that amplitude can be plotted as a function of time or anomaly, measured in number of orbits. The system being homogeneous, this amplitude should be compared to the initial amplitude one, or the amplitude corresponding to an initial speed of one.

Results are qualitatively, and even quantitatively in most cases, the same for initial speed or initial deviation. The results shown in Fig. 12 correspond to the in-plane, initial speed case, which is the most critical. Out-of-plane modes are not shown because all

remain bounded, except for the first. Four modes are chosen, which correspond to the four different behaviors observed.

All modes show-short period oscillations of their amplitudes, together with a longer-term evolution. The oscillations are due to the orbital and libration frequencies in the forcing terms. The amplitudes for the first mode, the straight line, grow steadily. This is not a problem because it only shows a perturbation of the libration: The change in the libration period, once linearized, is seen as a steady growth. Note that the time equation for mode 1 in-plane is precisely the variational equation of the libration (2). Conversely, the time equation for mode 1 out-of- plane is the variational equation of the out-of-plane libration.[16]

The second mode, the C shape, shows a moderate growth for some intermediate values of θ_M, with maximum drift at about 55 deg, and decreasing afterward. This seems to be a resonance. Note that the scale is $\frac{1}{100}$th of the earlier one. There is no resonance for the out-of-plane oscillations. Even though the eigenfunctions and eigenvalues are the same, the coefficients in the time equations are different.

The third mode, the S shape, grows exponentially for all values of θ_M, faster as the amplitude increases and approaches the zero-tension area. The fourth mode, the W shape, shows the same behavior, though less intense.

The fifth and higher modes remain bounded for the time computed. Note the smaller scale, which is the same as in the second mode. For out-of-plane oscillations, modes 2 and higher also show this kind of behavior.

In short, pendular libration is unstable for a free-end tether. However, the fastest growing mode takes about four orbits to develop, so that there is enough time to complete the injection, which required about 1.5 for maximum life.

The same computations are made after adding a small mass, $m = 3$ kg. All modes now remain bounded except two out-of-plane modes, the second, the C shape, and the third, the S shape, which are shown in Fig. 13 for the initial speed solution. The initial deviation solution is analogous, but tamer. The second mode shows the resonant behavior found in the free-end second mode for the same angle of 55 deg. It is slightly more intense and out-of-plane. The third mode shows the same high-amplitude low-tension behavior as the in-plane free-end third mode, but is remarkably subdued. Note the lower scale. The straight modes are unstable as before, but this is not a concern. Stability has generally improved, and most unstable modes now remain bounded, but there are still two unstable modes and one resonance has become slightly worse.

Other masses are tried to attempt to reduce this resonance. For $m = 5$, all modes are bounded, except the second in-plane. For

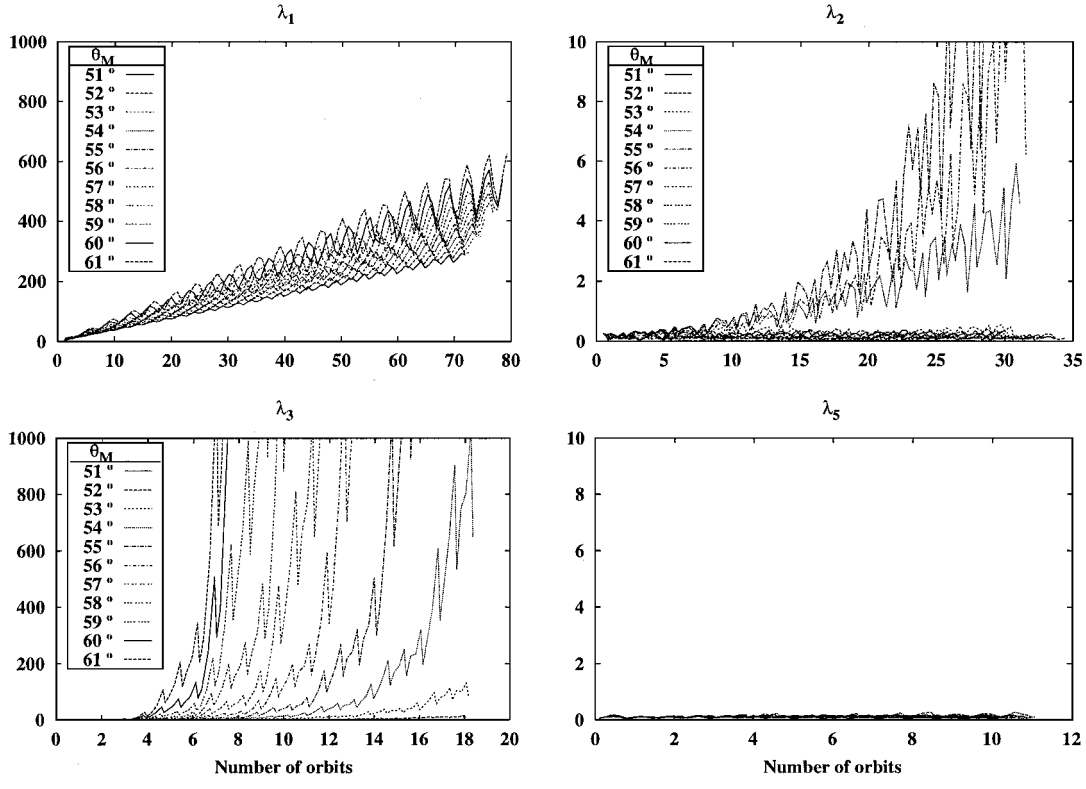

Fig. 12 In-plane, initial speed *Z* mode amplitudes with free end.

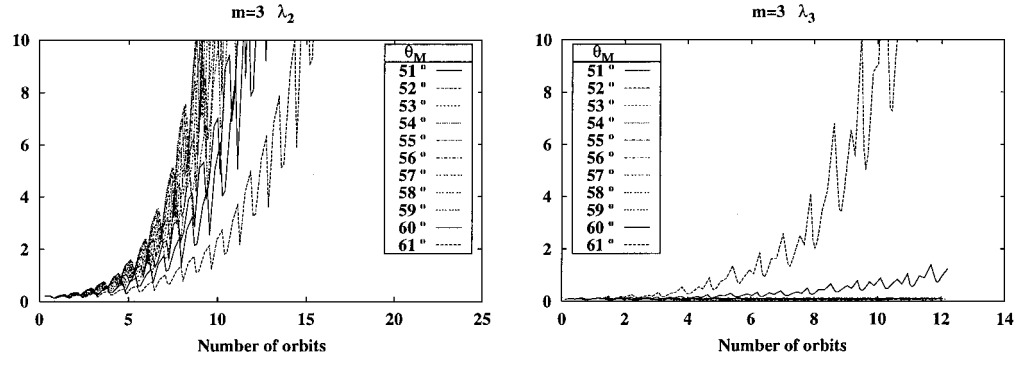

Fig. 13 Out-of-plane unstable *E* modes with *m* = 3.

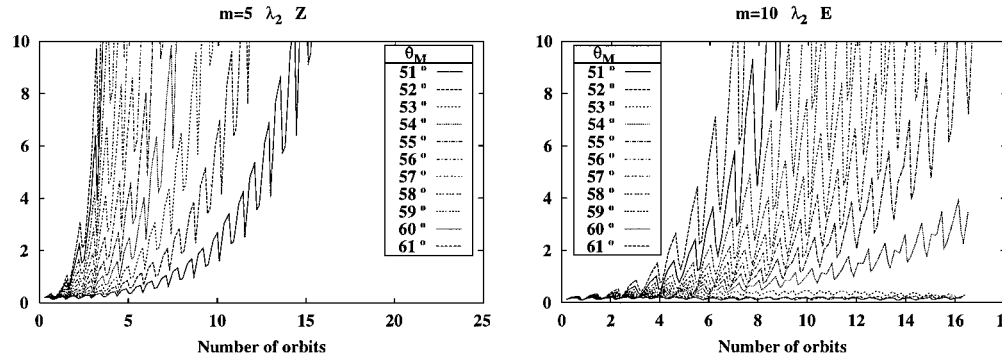

Fig. 14 Unstable mode amplitude λ_2 for m = 5 (in-plane) and m = 10 kg (out-of-plane).

Table 1 Eigenvalues and end mass

m, kg	λ_2	λ_3	λ_4	λ_5	λ_6
0	5.43	13.45	25.03	40.17	58.87
1	6.57	19.60	41.01	70.93	109.38
2	7.71	24.67	52.77	92.09	142.62
3	9.39	31.75	68.92	120.94	187.81
4	9.93	33.99	73.98	129.97	201.94
5	10.98	38.28	83.70	147.28	229.03
6	11.98	42.35	92.92	163.70	254.70
10	15.56	56.84	125.59	221.85	345.60
15	19.25	71.69	159.05	281.36	438.61

$m = 10$, the second mode is also unstable, but now for the out-of-plane oscillation, as shown in Fig. 14. For higher values of m, for example, $m = 15$ kg, all modes remain bounded.

This curious behavior is explained by the evolution of the eigenvalues, shown in Fig. 10 and Table 1. For $m = 0$, eigenvalues $\lambda_2 = 5.43$, $\lambda_3 = 13.45$, and $\lambda_4 = 25.03$ are unstable, one due to resonance and the other two due to diminishing tension. For $m = 3$, λ_2 has grown to 9.39, which is between the two earlier instabilities, and thus keeps the resonance, and even gets worse due to the proximity of the other instability. The third has grown enough to clear the worst of the instability area encompassing 13.45 and 25.03 and only shows a moderate growth. This recalls the stability regions of the Mathieu equation, which is not surprising because the eccentricity resulting from the slingshot is small. As eigenvalues change, they get in and out of different unstable zones. For lower masses, the eigenvalues are so close to those of $m = 0$ that their behavior is the same, especially in the wider, lower-frequency zones. As the masses increase to 5 and 10, λ_2 is still within the unstable area of the third and fourth free-end modes, as shown in Fig. 14. Finally, for $m = 15$, it has grown enough to clear it, and all modes are bounded.

All in all, $m = 3$ seems to be a good compromise and a good improvement from the free-end case, unless we are ready to increase the end mass up to $m = 15$ kg.

Conclusions

Leaving a second mass attached to the otherwise free end of a tether in a slingshot orbital injection is beneficial:

1) It achieves a higher orbit and longer satellite lifetime even for small values of the mass.

2) In low orbits, the effect of an end mass is dramatic: It can even double the one-cut lifetime.

3) Sensitivity to cut parameters is small, except for ν_c.

4) It can improve the stability of the libration, which is very unstable with a free end.

5) It does not need additional weight.

Still, because the new mass can create its own set of resonances, stability must be investigated in each case. If resonances are found, they can be avoided by changing m or L so that the eigenvalues are out of the unstable zones. This is a low-cost solution that can be easily implemented using as end mass some part of the releasing hardware, which is expendable in most cases. On the other hand, this would require redesign of existing and proven hardware, and would limit the choice of an optimum m.

Acknowledgments

The authors would like to thank the Spanish Agencies Dirección General de Investigatión Científica y Técnica and Oficina de Transferencia de Tecnología for their support under Grants PB94-0417-C03-02 and PB97-0574-C04-04 and Enrico Lorenzini of Harvard–Smithsonian Center for Astrophysics for his assistance.

References

[1]Cosmo, M., and Lorenzini, E., *Tethers in Space Handbook*, 3rd ed., Smithsonian Astrophysical Observatory, Cambridge, MA, 1997.

[2]Bangham, M., Lorenzini, E., and Vestal, L., "Tether Transportation System Study," NASA TR TP-1998-206959, March 1998.

[3]Lorenzini, E., Cosmo, M., Kaiser, M., Bangham, M., Dionne, H., Vonderwell, D., and Johnson, L., "Mission Analysis of a Tethered System for LEO to GEO Orbital Transfers," *Spaceflight Mechanics 1998*, Vol. 99-I Advances in the Astronautical Sciences, Univelt, Inc., Monterey, CA, Feb. 1998, pp. 3–20.

[4]James, H., "The BOLAS Mission," *Proceedings of the Tether Technology Interchange Meeting*, edited by J. Harrison, CP-1998-206900, NASA, 1997, pp. 71–102.

[5]Harrison, J. K., "SEDS/SEDSAT Project Overview," *Proceedings of the Fourth International Conference on Tethers in Space*, Smithsonian Inst., Washington, DC, Vol. 1, 1995, pp. 85–93.

[6]Kruijff, M., and van der Heide, E. J., "The YES Satellite: a Tethered Momentum Transfer in the GTO Orbit," *Proceedings of the Tether Technology Interchange Meeting*, edited by J. Harrison, CP-1998-206900, NASA, 1997, pp. 131–148.

[7]Gates, S. S., Koss, S. M., and Zedd, M. F., "Advanced Tether Experiment Deployment Failure," American Astronautical Society, AAS Paper 99-413, Aug. 1999.

[8]Bekey, I., and Penzo, P., "Tether Propulsion," *Aerospace America*, Vol. 24, No. 7, 1986, pp. 40–43.

[9]Kumar, K., Kumar, R., and Misra, A., "Effects of Deployment Rates and Librations on Tethered Payload Raising," *Journal of Guidance, Control, and Dynamics*, Vol. 15, No. 5, 1992, pp. 1230–1235.

[10]Sanz-Andrés, A., and Meseguer, J., "The Programme of Small Satellites of the Universidad Politécnica de Madrid," *Conferencia International sobre Pequeños Satélites: Misiones y Tecnología*, Inst. Nacional de Técnica Aerospacial, Madrid, 1996, pp. 1.11–1.17.

[11]Lorenzini, E., Gullahorn, G., Cosmo, M., Ruiz, M., and Peláez, J., "Orbital Injection of the SEDSAT Satellite," Annual Rept. for NASA Grant NAG8-1046, Smithsonian Astrophysical Observatory, Cambridge, MA, 1996.

[12]Peláez, J., Ruiz, M., and Lorenzini, E., "Strategies for Maximizing a Satellite Lifetime by Tether-Mediated Orbital Injection," *Journal of Astronautical Sciences*, Vol. 45, No. 2, 1997, pp. 205–231.

[13]Ruiz, M., *Análisis Dinámico de Cables Espaciales (Tethers): Aplicaciones a la Dinámica Orbital*, Ph.D. Dissertation, Escuela Técnica Superior de Ingenieros Aeronáuticos, Univ. Politécnica de Madrid, Madrid, Dec. 1999.

[14]Ruiz, M., Peláez, J., and Lorenzini, E., "Stability of the Pendular Motion of a Tethered System in Elliptical Orbit," *Spacefight Mechanics 1996*, edited by G. Powell, R. Bishop, J. Lundberg, and R. Smith, No. 93-II, Advances in

the Astronautical Sciences, American Astronautical Society, Univelt, Inc., Monterey, CA, 1996, pp. 1553–1569.

[15]Peláez, J., "On the Dynamics of the Deployment of a Tether from an Orbiter. I—Basic Equations," *Acta Astronautica*, Vol. 36, No. 2, 1995, pp. 113–122.

[16]Beletsky, V., and Levin, E., *Dynamics of Space Tether Systems*, No. 83, Advances in the Astronautical Sciences, American Astronautical Society, San Diego, CA, 1993, pp. 78, 362, 379, 380, 382.

[17]Ruiz, M., and Peláez, J., "Slingshot Orbital Injection Revisited," *Spaceflight Mechanics 1999*, edited by R. H. Bishop, D. L. Mackison, R. D. Culp, and M. J. Evans, No. 102-II, Advances in the Astronautical Sciences, American Astronautical Society, Univelt, Inc., Monterey, CA, 1999, pp. 1381–1397.

[18]King-Hele, D., *Satellite Orbits in an Atmosphere: Theory and Applications*, Blackie and Son, Ltd., Glasgow and London, 1987, p. 60.

[19]Press, W., Teukolsky, S., Vetterling, W., and Flannery, B., *Numerical Recipes in C*, 2nd ed., Cambridge Univ. Press, Cambridge, England, U.K., 1992, pp. 420, 772.

[20]Schechter, H. B., "Dumbbell Librations in Elliptic Orbits," *AIAA Journal*, Vol. 2, No. 6, 1964, pp. 1000–1003.

[21]Modi, V., and Brereton, R., "Libration Analysis of a Dumbbell Satellite Using the WKBJ Method," *Journal of Applied Mechanics*, Vol. 33, No. 3, 1966, pp. 676–678.

[22]Brereton, R., and Modi, V., "On the Stability of Planar Librations of a Dumb-Bell Satellite in an Elliptic Orbit," *Journal of the Royal Aeronautical Society*, Vol. 70, No. 672, 1966, pp. 1098–1102.